Corrosion Science 53 (2011) 3688–3696

Contents lists available at ScienceDirect

Corrosion Science

journal homepage: www.elsevier.com/locate/corsci

Effect of 4-(*N*,*N*-diethylamino)benzaldehyde thiosemicarbazone on the corrosion of aged 18 Ni 250 grade maraging steel in phosphoric acid solution

T. Poornima [a], Jagannath Nayak [b], A. Nityananda Shetty [c,*]

[a] Department of Science and Humanities, PESIT, Bangalore 560085, India
[b] Department of Metallurgical and Materials Engineering, National Institute of Technology Karnataka, Surathkal, Srinivasnagar 575025, Karnataka, India
[c] Department of Chemistry, National Institute of Technology Karnataka, Surathkal, Srinivasnagar 575025, Karnataka, India

ARTICLE INFO

Article history:
Received 20 December 2010
Accepted 4 July 2011
Available online 20 July 2011

Keywords:
A. Steel
B. EIS
B. SEM
C. Acid corrosion

ABSTRACT

4-(*N*,*N*-diethylamino)benzaldehyde thiosemicarbazone (DEABT) was studied for its corrosion inhibition property on the corrosion of aged 18 Ni 250 grade maraging steel in 0.67 M phosphoric acid at 30–50 °C by potentiodynamic polarization, EIS and weight loss techniques. Inhibition efficiency of DEABT was found to increase with the increase in DEABT concentration and decrease with the increase in temperature. The activation energy E_a and other thermodynamic parameters (ΔG^0_{ads}, ΔH^0_{ads}, ΔS^0_{ads}) have been evaluated and discussed. The adsorption of DEABT on aged maraging steel surface obeys the Langmuir adsorption isotherm model and the inhibitor showed mixed type inhibition behavior.

1. Introduction

Maraging steels are special class of ultra high strength steels that differ from conventional steels in that they are hardened by a metallurgical reaction that does not involve carbon [1]. These alloys derive their high strength from the age hardening of low carbon, Fe–Ni martensitic matrix [2]. These gray and white steels are characterized with high ductility, formability, corrosion resistance, high temperature strength and ease of fabrication, weldability and maintenance of invariable size even after heat treatment [3]. These steels have emerged as alternative materials to conventionally used quenched and tempered steels for advanced technologies such as aerospace, nuclear and gas turbine applications. They frequently come into contact with acids during cleaning, pickling, descaling, acidizing, etc. According to the available literature, 18 Ni maraging steel, when exposed to atmosphere, undergoes more or less uniform corrosion and gets completely covered with rust [4]. The pits formed in this were found to be shallower than in high strength steels [5]. The corrosion of maraging steel in slightly acidic radioactive water in the presence and absence of chloride ions, at the corrosion potential depended on pH, and the intermediates remained on the maraging steel surface in the active region, favoring the passivity [6]. The effect of carbonate ions in slightly alkaline medium on the corrosion of maraging steel was studied by Bellanger [7]. Reports are also available, indicating that the critical and passive current densities increase as the structure is varied from one of being fully annealed to one of fully aged [8]. Maraging steels were found to be less susceptible to hydrogen embrittlement than the common high strength steels owing to the significantly low diffusion of hydrogen in them [9].

Phosphoric acid solutions are used in pickling of delicate and costly components and precision items where re-rusting after pickling has to be avoided [10]. Phosphoric acid has the unique property of dissolving rust quickly while etching iron very slowly. The other advantage of phosphoric acid is that it leaves fine iron phosphate coating on the surface of the alloy, preventing further corrosion. However, the iron phosphate coating is not very thick and durable. Some additional protection like use of corrosion inhibitor is necessary. Phosphoric acid shows corrosiveness on steel and steel alloys. However no literature seems to be available on the corrosion behavior of maraging steel in the acid medium except our own previous study [11]. Although the maraging steel alloys, in general, are corrosion resistant compared to conventional steels, our previous study has revealed substantial corrosion of aged maraging steel in phosphoric acid medium. We have earlier reported the use of 3,4-dimethoxy benzaldehyde thiosemicarbazone as an effective inhibitor for aged 18 Ni 250 grade maraging steel in sulfuric acid medium [12]. The present work addresses the assessment of corrosion inhibition of aged 18 Ni 250 grade maraging steel in phosphoric acid medium using DEABT as inhibitor.

The majority of the well known inhibitors are organic compounds containing hetero-atoms, such as O, N, or S and multiple bonds or aromatic rings, which allow an adsorption on the metal surface through lone pair of electrons and/or pi electrons present

* Corresponding author. Tel.: +91 824 2474200, mobile: +91 9448779922; fax: +91 824 2474033.
E-mail address: nityashreya@gmail.com (A. Nityananda Shetty).

0010-938X/$ - see front matter © 2011 Elsevier Ltd. All rights reserved.
doi:10.1016/j.corsci.2011.07.014

in these molecules [13,14]. The inhibition efficiency increases in the order O < N < S < P [15]. The molecules that contain both nitrogen and sulfur in their structures are of particular importance, since they provide an excellent inhibition effect compared with the compounds that contain only sulfur or nitrogen [16]. Thiosemicarbazones and their derivatives have continued to be a subject of extensive investigation in chemistry and biology owing to their broad spectrum of anti-tumor [17], antimalarial [18], antiviral [19], antibacterial [20], antifungal [21] and many other applications including corrosion inhibition of metals [22–25].

2. Experimental

2.1. Materials

The maraging steel samples (M 250 grade) in aged condition were taken from plates. The solution-annealed and air-cooled plates were subjected to aging treatment at 480 ± 5 °C for 3 h and air cooled. Chemical composition of 18 Ni 250 grade aged maraging steel samples is given in Table 1. Test coupons in the cylindrical form were cut from the plate and sealed with epoxy resin in such a way that the area exposed to the medium was 0.503 cm^2. These coupons were polished as per standard metallographic practice – belt grinding followed by abrading on emery papers, finally on polishing wheel using legated alumina to obtain mirror finish. Then it was degreased with acetone, washed with double distilled water and dried before immersing in the corrosion medium.

The inhibitor DEABT was synthesized as per the reported procedure [26] in a single step reaction between 4-(diethylamino) benzaldehyde with thiosemicarbazide. An equimolar ethanolic mixture of 4-(diethylamino) benzaldehyde and thiosemicarbazide in a round bottom flask was refluxed on a hot water bath for about 60 min. The light yellow colored product formed was separated by filtration, recrystallised from ethanol and characterized by elemental analysis and melting point. Elemental analysis: found (calculated): C 57.9 (57.6), H 5.5 (5.6), N 22.6 (22.4), S 13.1 (12.8). The structure of the molecule is given below.

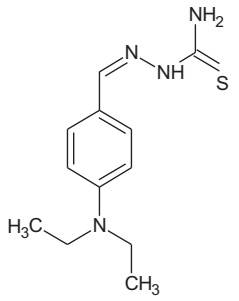

2.2. Medium

Standard 0.67 M phosphoric acid solution was prepared by diluting Analar grade 85% phosphoric acid with double distilled water and standardized. The solutions of the inhibitor in the concentration range of 2.0×10^{-4} to 12×10^{-4} M were prepared in standard 0.67 M phosphoric acid. Experiments were carried out using calibrated thermostat at temperatures 30, 35, 40, 45 and 50 °C (±0.5 °C).

Table 1
Composition of the aged maraging steel specimen.

Element	Composition (wt. %)	Element	Composition (wt. %)
C	0.015	Ti	0.52
Ni	18.19	Al	0.11
Mo	4.82	Mn	0.1
Co	7.84	P	0.01
Si	0.1	S	0.01
O	30 ppm	N	30 ppm
H	2.0 ppm	Fe	Balance

2.3. Electrochemical measurements

Electrochemical measurements were carried out using an electrochemical work station, Auto Lab 30, GPES software and FRA software. Tafel measurements and EIS measurements were carried out using conventional three-electrode Pyrex glass cell with platinum counter electrode as the auxiliary electrode and saturated calomel electrode (SCE) as reference electrode. All the values of potential are referred to the SCE. The Tafel polarization studies were carried out immediately after the EIS studies on the same electrode without any further surface treatment.

2.3.1. Tafel polarization studies

Finely polished and dried maraging steel specimens were exposed to the corrosion medium of 0.67 M phosphoric acid in the presence of different concentrations of inhibitor at different temperatures and allowed to establish a steady state open circuit potential (OCP). The potentiodynamic current–potential curves were recorded by polarizing the specimen to −250 mV cathodically and +250 mV anodically with respect to OCP at a scan rate of 1 mV s^{-1}.

2.3.2. Electrochemical impedance spectroscopy (EIS) studies

In EIS technique, a small amplitude ac signal of 10 mV and frequency spectrum from 100 kHz to 0.01 Hz was impressed at the OCP, and the impedance data were analyzed using Nyquist plots. The charge transfer resistance, R_{ct} was extracted from the diameter of the semicircle in the Nyquist plot.

2.3.3. Weight loss method

Finely polished and dried cylindrical maraging steel specimens of dimension 0.503 $cm^2 \times 1.5$ cm were weighed in a digital balance with sensitivity of 0.0001 mg and immersed in 0.67 M phosphoric acid solution in the absence and presence of different concentrations of the inhibitor at different temperatures. After 3 h the specimens were removed from the acid solution, the surface was thoroughly cleaned, dried and weighed. The weight loss was calculated as the difference in weight of the specimen before and after immersion in the corrosion medium.

In all the above measurements, at least three similar results were considered, and their average values are reported.

2.3.4. Scanning electron microscopic (SEM) analysis

The SEM images were recorded using JEOL JSM – 6380 LA analytical scanning electron microscope.

3. Results and discussion

3.1. Tafel polarization measurement

Fig. 1 shows the potentiodynamic polarization curves for the corrosion of aged maraging steel in 0.67 M phosphoric acid containing different concentrations of DEABT, at 30 °C. Similar plots were obtained at other temperatures also. The electrochemical parameters such as corrosion potential (E_{corr}), corrosion current density (i_{corr}), corrosion rate (υ_{corr}) and cathodic Tafel slope (b_c) associated with the polarization measurements for the alloy at different temperatures in the presence of different concentrations of DEABT are summarized in Table 2. Since the linear portion of the

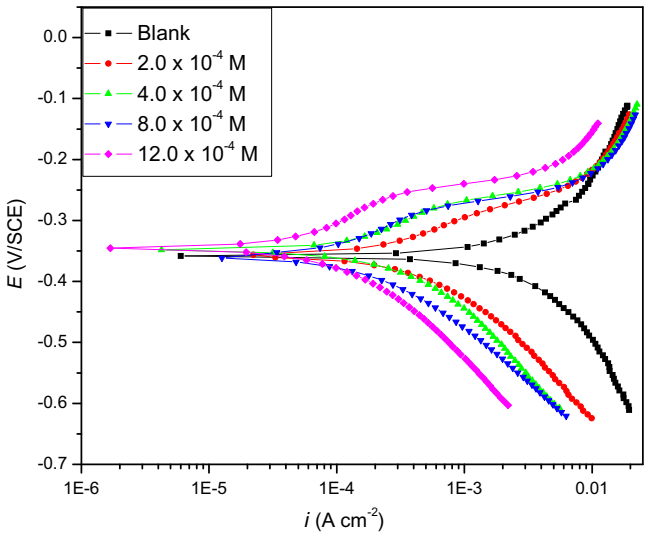

Fig. 1. Tafel polarization curves for the corrosion of aged maraging steel in 0.67 M phosphoric acid containing different concentrations DEABT.

anodic region is not well defined, the corrosion current densities in all the above cases were determined by the extrapolation of cathodic Tafel slopes to the respective corrosion potentials.

The surface coverage θ of the inhibitor at different inhibitor concentrations were calculated from the equation:

$$\theta = \frac{i_{corr} - i_{corr_{(inh)}}}{i_{corr}}, \quad (1)$$

where i_{corr} and $i_{corr(inh)}$ are the corrosion current densities in the absence and in the presence of inhibitor respectively.

Inhibition efficiency was then calculated using the equation:

$$\eta(\%) = \theta \times 100. \quad (2)$$

The inhibition efficiency (η) of DEABT is also given in Table 2. The data in the Table 2 clearly show that the DEABT effectively decreases the corrosion current density of the aged maraging steel, even when added in small concentrations. Inhibition efficiency increases with the increase in the inhibitor concentration up to an optimum value. There after the increase in the inhibitor concentration resulted in negligible increase in inhibition efficiency. The maximum quantity of the inhibitor reported in Table 2 corresponds to the optimum concentration of the inhibitor. The presence of inhibitor does not cause any significance shift in the E_{corr} value. This implies that the inhibitor, DEABT, acts as a mixed type inhibitor, affecting both anodic and cathodic reactions [27]. According to Riggs and others [28], if the displacement in corrosion potential is more than ±85 mV/SCE with respect to the corrosion potential of the blank, the inhibitor can be considered as a cathodic or anodic type. But the maximum displacement in the present case is less than 20 mV/SCE, which indicates that DEABT is a mixed type inhibitor. According to Cao [29] if the shift in E_{corr} is negligible, the inhibition is most probably caused by a geometric blocking effect of the adsorbed inhibitive species on the surface of corroding metal.

Fig. 1 indicates that the cathodic polarization curves are parallel and cathodic Tafel slope b_c changes only slightly with the increase in the inhibitor concentration. This suggests that the reduction mechanism is not affected by the presence of inhibitor [30,31] and hence the hydrogen evolution is slowed down by the surface blocking effect of the inhibitor. The variation in anodic Tafel slope b_a may be due to the adsorption of phosphate ions/or inhibitor molecules on the alloy surface [32]. This indicates that the inhibitive action of DEABT may be considered due to the adsorption and formation of barrier film on the electrode surface. The barrier film formed on the metal surface reduces the probability of both the anodic and cathodic reactions. Thus, the inhibitor, DEABT can be regarded as a mixed type of inhibitor.

It is seen from Fig. 1 that at the working electrode potentials, greater than −250 mV/SCE, on the anodic polarization region, the current–potential characteristics do not change in the presence of the inhibitor. Above this potential there is a sharp increase in

Table 2
Results of Tafel polarization studies for the corrosion of aged maraging steel in 0.67 M phosphoric acid in the presence of different concentrations of DEABT at different temperatures.

Temperature (°C)	Inhibitor (mM)	E_{corr} (V/SCE)	i_{corr} (mA cm^{-2})	$-b_c$ (V dec^{-1})	υ_{corr} (mM y^{-1})	η (%)
30	0.0	−0.354 ± 2.5	1.431 ± 0.12	0.185 ± 4.3	16.59 ± 1.2	
	0.2	−0.370 ± 1.3	0.522 ± 0.06	0.172 ± 3.2	6.05 ± 0.6	63.55
	0.4	−0.355 ± 3.3	0.208 ± 0.03	0.174 ± 2.7	2.41 ± 0.3	85.48
	0.8	−0.351 ± 3.6	0.176 ± 0.07	0.179 ± 3.1	2.04 ± 0.7	87.71
	1.2	−0.347 ± 2.3	0.141 ± 0.01	0.183 ± 2.1	1.63 ± 0.1	90.18
35	0.0	−0.371 ± 1.8	1.586 ± 0.09	0.185 ± 5.2	18.40 ± 0.9	
	0.2	−0.366 ± 4.2	0.636 ± 0.04	0.201 ± 4.2	7.38 ± 0.4	59.89
	0.4	−0.351 ± 3.2	0.295 ± 0.06	0.200 ± 5.1	3.42 ± 0.6	81.41
	0.8	−0.352 ± 2.5	0.241 ± 0.04	0.189 ± 1.3	2.80 ± 0.4	84.78
	1.2	−0.350 ± 2.5	0.178 ± 0.02	0.179 ± 2.8	2.07 ± 0.2	88.75
40	0.0	−0.371 ± 3.1	1.862 ± 0.05	0.198 ± 3.3	21.60 ± 0.5	
	0.2	−0.370 ± 3.6	0.897 ± 0.01	0.211 ± 4.1	10.40 ± 0.1	51.85
	0.4	−0.363 ± 4.3	0.402 ± 0.03	0.198 ± 5.2	4.66 ± 0.3	78.43
	0.8	−0.348 ± 3.1	0.328 ± 0.02	0.191 ± 4.4	3.80 ± 0.2	82.41
	1.2	−0.350 ± 1.6	0.247 ± 0.01	0.185 ± 5.2	2.87 ± 0.1	86.71
45	0.0	−0.366 ± 2.2	2.180 ± 0.02	0.188 ± 3.2	25.29 ± 0.2	
	0.2	−0.358 ± 2.5	1.100 ± 0.02	0.214 ± 3.1	12.76 ± 0.2	49.55
	0.4	−0.356 ± 3.1	0.539 ± 0.03	0.198 ± 4.1	6.25 ± 0.3	75.29
	0.8	−0.349 ± 2.4	0.418 ± 0.04	0.199 ± 4.1	4.85 ± 0.4	80.82
	1.2	−0.347 ± 4.2	0.312 ± 0.06	0.188 ± 3.6	3.62 ± 0.6	85.69
50	0.0	−0.346 ± 4.1	2.430 ± 0.01	0.191 ± 4.2	28.19 ± 0.1	
	0.2	−0.358 ± 2.4	1.284 ± 0.03	0.214 ± 4.2	14.90 ± 0.3	47.14
	0.4	−0.356 ± 4.2	0.652 ± 0.02	0.206 ± 5.1	7.56 ± 0.2	73.18
	0.8	−0.349 ± 2.2	0.581 ± 0.05	0.199 ± 4.9	6.73 ± 4.9	76.13
	1.2	−0.342 ± 1.6	0.474 ± 0.01	0.184 ± 0.01	5.50 ± 4.5	80.49

current density with the increase in the potential, as indicated by the flat region on the anodic curve. This potential can be defined as desorption potential [33]. This phenomenon may be understood by considering the adsorption of the inhibitor molecules on the alloy surface and desorption of the inhibitor molecules due to the dissolution of the metal in the corrosion medium; both taking place simultaneously. In this case, the desorption rate of the inhibitor is higher than its adsorption rate, resulting in the increase in the corrosion current with the increase in the potential [34]. At still higher polarization potential the anodic current density change drastically, resulting in sharp increase in Tafel slope.

3.2. Electrochemical impedance spectroscopy

The Nyquist plots obtained for the aged samples of maraging steel in 0.67 M phosphoric acid in the presence of different concentrations of DEABT at 30 °C are shown in Fig. 2. Similar plots were obtained at other temperatures also.

The shapes of the impedance plots for the alloy in the presence of the inhibitor are quite similar to that in the absence of the inhibitor. The presence of the inhibitor only increases the impedance without changing other aspects of the behavior. These results are in agreement with the results of polarization measurements that the inhibitor does not alter the mechanism of electrochemical reactions responsible for corrosion. The inhibition action of DEABT is primarily through its adsorption on the metal surface [35], forming a barrier film between the metal surface and the corrosion medium. The Nyquist plots, both in the absence and presence of the inhibitor are characterized by two time constants, with a depressed capacitive semicircle at high frequency (HF) region followed by an inductive loop at low frequency (LF) region. These are not perfect semicircles, because the Nyquist plots obtained in the real system represent a general behavior where the double layer at the metal solution interface does not behave as an ideal capacitor [36]. The depressed capacitive loop with its center below the real axis often refers to the frequency dispersion of interfacial impedance which has been attributed to the roughness and non-homogeneity of the solid surfaces, and also to the adsorption of inhibitors [37]. The HF capacitive loop is attributed to the charge transfer of the corrosion process and time constant of the electric double layer [38]. The LF inductive loop can be attributed to the relaxation process obtained by the adsorbed phosphate ions and protons [39]. It may also be attributed to the re-dissolution of the passivated surface at the low frequencies [40]. In the present case, the low frequency inductive loop in the inhibitor free acid medium can be attributed to the surface dissolution process at low frequencies. The low frequency inductive loop in the inhibited acid solution might be attributed to the surface dissolution at low frequency, indicating that the alloy still dissolved by the direct charge transfer at the inhibitor adsorbed steel surface [41].

Based on the shape of Nyquist plots, the equivalent circuit used is as given in Fig. 3, which has been previously used to model iron/acid interface [42]. In this equivalent circuit R_s is the solution resistance and R_{ct} is the charge transfer resistance. R_L and L represent the inductive elements. This also consists of constant phase element, CPE (Q) in parallel to the parallel resistors R_{ct} and R_L, and the later is in parallel with the inductor L. The surface roughness, degree of polycrystallinity and also the anion adsorption on the surface leads to the capacitance dispersion at solid electrodes and hence the real iron/acid interface system deviates from ideal capacitive behavior, which can be empirically represented by the CPE [43]. R_s represent the solution resistance due to the ohmic resistances of corrosion product films and the solution enclosed between the working electrode and the reference electrode. R_{ct} represents the charge transfer resistance whose value is a measure of electron transfer across the surface and is inversely proportional to the corrosion rate [44].

The charge transfer resistance R_{ct} and double layer capacitance C_{dl} were determined by the analysis of Nyquist plots and their values are given in Table 3. As can be seen from Table 3, R_{ct} value increases and C_{dl} value decreases with the increase in the concentration of DEABT, indicating that inhibitor molecules function by adsorption at the metal/solution interface, leading to the formation of a protective film on the alloy surface.

The inhibition efficiencies in the presence of different concentrations of inhibitors were calculated from the charge transfer resistance values, according to the equation,

$$\eta(\%) = \left(\frac{R_{ct} - R_{ct}^0}{R_{ct}}\right) \times 100, \quad (3)$$

where R_{ct} and R_{ct}^0 represent the charge transfer resistance in the presence and absence of the inhibitor. The inhibition efficiency values obtained by the electrochemical impedance method are in good agreement with the ones obtained by Tafel's polarization studies.

3.3. Weight loss measurements

Weight loss method of monitoring the corrosion rate and calculating the inhibition efficiency is useful because of its reliability. The percentage inhibition efficiency of DEABT was calculated from the equation:

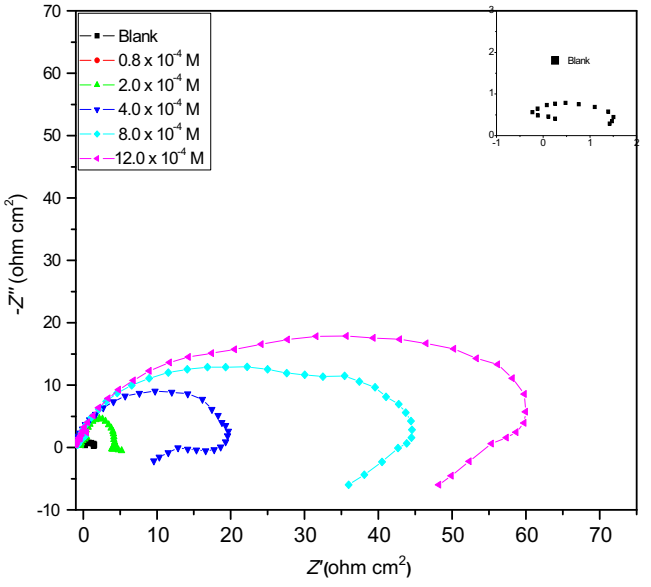

Fig. 2. Nyquist plots for the corrosion of aged maraging steel in 0.67 M phosphoric acid containing different concentrations of DEABT.

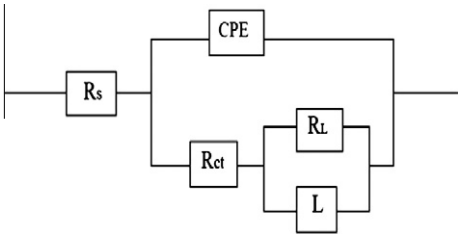

Fig. 3. Equivalent circuit used to fit experimental EIS data for the corrosion of aged maraging steel specimen in 0.67 M phosphoric acid with and without inhibitor.

Table 3
EIS data for the corrosion of aged maraging steel in 0.67 M phosphoric acid in the presence of different concentrations of DEABT at different temperatures.

Temperature (°C)	Inhibitor (mM)	R_{ct} (ohm cm^2)	C_{dl} (mF cm^{-2})	η (%)
30	0.0	2.6 ± 0.2	25.2 ± 3.4	
	0.2	8.8 ± 1.1	4.9 ± 0.4	70.45
	0.4	23.4 ± 2.2	3.2 ± 0.4	88.89
	0.8	41.8 ± 2.3	3.0 ± 0.7	93.78
	1.2	53.4 ± 2.2	2.0 ± 0.8	95.13
35	0.0	1.9 ± 2.1	71.3 ± 10.4	
	0.2	5.3 ± 2.1	4.4 ± 1.0	63.67
	0.4	14.5 ± 1.5	3.4 ± 0.8	86.62
	0.8	23.6 ± 2.4	2.7 ± 0.6	91.78
	1.2	38.2 ± 3.2	2.0 ± 0.8	94.92
40	0.0	1.5 ± 0.5	95.0 ± 14.6	
	0.2	3.7 ± 1.6	3.8 ± 1.1	59.89
	0.4	10.7 ± 2.4	2.3 ± 0.8	85.98
	0.8	15.6 ± 2.8	3.6 ± 0.8	90.36
	1.2	23.7 ± 3.7	3.6 ± 0.6	93.67
45	0.0	1.0 ± 0.4	892.6 ± 25.8	
	0.2	2.4 ± 1.1	11.9 ± 2.1	57.45
	0.4	5.2 ± 1.0	4.0 ± 0.8	80.86
	0.8	8.6 ± 2.3	3.9 ± 0.8	88.41
	1.2	10.2 ± 3.1	2.1 ± 0.6	90.22
50	0.0	0.9 ± 0.3	1270.3 ± 45.3	
	0.2	1.9 ± 1.4	9.5 ± 2.4	51.58
	0.4	4.0 ± 2.2	5.5 ± 1.5	76.71
	0.8	5.4 ± 2.6	4.6 ± 1.2	82.90
	1.2	7.5 ± 3.1	3.3 ± 0.7	87.77

$$\eta(\%) = \frac{W_0 - W}{W_0} \times 100, \tag{4}$$

where W_0 and W are the weight losses of the maraging steel per unit area in the absence and presence of inhibitor, respectively.

Table 4 lists the inhibition efficiencies obtained by weight loss measurements in 0.67 M phosphoric acid in the presence of different concentrations of DEABT at different temperatures. From the Table it is seen that the inhibition efficiency values are in good agreement with the ones obtained by electrochemical studies.

3.4. Effect of temperature

The corrosion of a metal in the presence of an inhibitor involves many changes occurring on the metal surface, such as rapid etching and desorption of the inhibitor and the inhibitor itself, in some cases, may undergo decomposition and/or rearrangement [42]. Therefore the effect of temperature on the inhibited acid-metal reaction is highly complex. However, the study of the effect of temperature on the corrosion system facilitates the calculation of many thermodynamic functions for the inhibition and/or the adsorption processes which contribute in determining the type of adsorption of the studied inhibitors.

From Table 2, it can be seen that the inhibition efficiency decreases with the increase in temperature which indicates the probable desorption of inhibitor molecules from the surface of the alloy as the temperature increases [45]. This is suggestive of physisorption of DEABT molecules on the alloy surface [46]. But the decrease in inhibition efficiency with the increase in temperature becomes gradual at higher concentrations of the inhibitor.

Table 4
Inhibition efficiency of DEABT for the corrosion of aged maraging steel in 0.67 M phosphoric acid as determined by weight loss method.

Inhibitor (mM)	η (%)				
	30 °C	35 °C	40 °C	45 °C	50 °C
0.2	68.48	62.46	56.47	54.45	50.54
0.4	86.00	85.62	82.77	78.82	74.75
0.8	90.46	87.78	85.44	83.41	79.98
1.2	92.17	91.09	90.63	88.24	86.72

The activation energy (E_a) for the corrosion process in the presence and absence of the inhibitor, DEABT, were calculated using Arrhenius law Eq. (5) [13].

$$\ln v_{corr} = B - \frac{E_a}{RT} \tag{5}$$

where B is a constant which depends on the metal type and R is the universal gas constant. The plot of ln υ_{corr} versus reciprocal of absolute temperature, $1/T$, gives a straight line with slope = $-E_a/R$, from which the activation energy for the corrosion process can be calculated. The Arrhenius plots for the corrosion of aged maraging steel in the phosphoric acid containing DEABT are shown in Fig. 4.

The entropy of activation ($\Delta H^{\#}$) and enthalpy of activation ($\Delta S^{\#}$) for the corrosion of alloy were calculated from the transition state theory Eq. (6) [13].

$$v_{corr} = \frac{RT}{Nh} \exp\left(\frac{\Delta S^{\#}}{R}\right) \exp\left(\frac{-\Delta H^{\#}}{RT}\right) \tag{6}$$

where h is Planck's constant and N is Avagadro's number. A plot of ln (υ_{corr}/T) versus $1/T$ gives a straight line with the slope = $-\Delta H^{\#}/R$ and the intercept = $\ln(R/Nh) + \Delta S^{\#}/R$. The plots of $\ln(\upsilon_{corr}/T)$ versus $1/T$ for the aged maraging steel in the presence of different concentrations of DEABT are shown in Fig. 5. The calculated values of E_a, $\Delta H^{\#}$ and $\Delta S^{\#}$ are given in Table 5.

The chemically stable surface active inhibitors increase the energy of activation and decrease the surface area available for corrosion [47]. From Table 5 it is seen that the value of activation energy (E_a) for the corrosion of the alloy in the phosphoric acid solution in the presence of the inhibitor is higher than that in the absence of the inhibitor. Also, the extent of increase is proportional to the inhibitor concentration, indicating that the energy barrier for the corrosion reaction increases with the increase in the concentration of DEABT. The increase in the activation energy E_a may be considered to be due to the physical adsorption [48] of the inhibitor, which results in the increase in surface coverage with the increase in the concentration of the inhibitor. The values at different temperatures also reveal that the inhibition efficiency decreases with the increase in temperature. This may be due to the decrease in the adsorption of the inhibitor on the alloy surface as the temperature increases and a corresponding increase in the

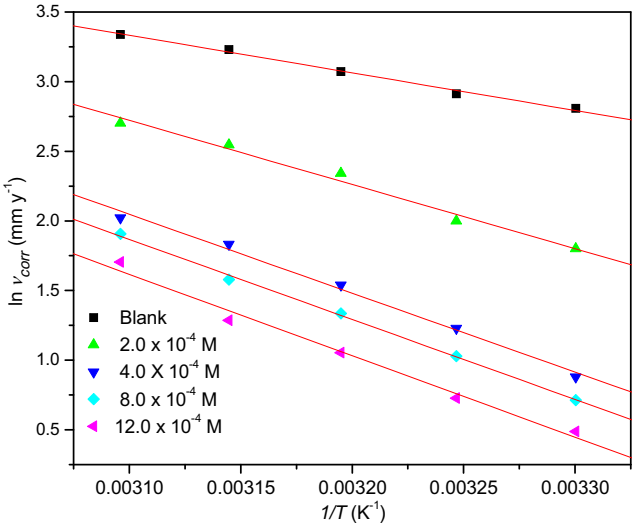

Fig. 4. Arrhenius plots for the corrosion of aged maraging steel in 0.67 M phosphoric acid containing different concentrations of DEABT.

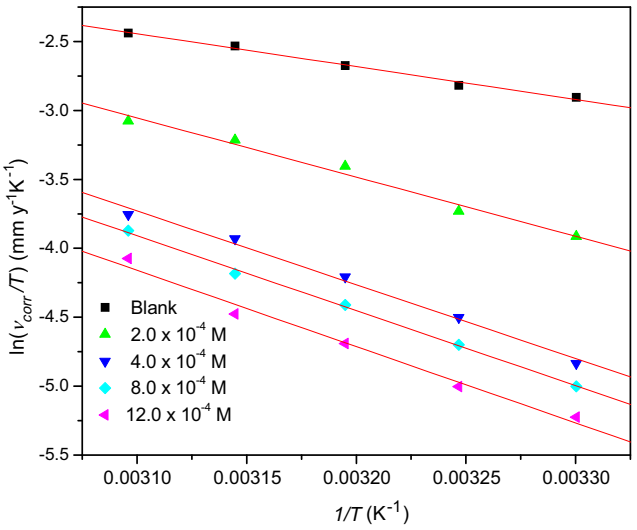

Fig. 5. $\ln(\upsilon_{corr}/T)$ versus $1/T$ for the corrosion of aged maraging steel in 0.67 M phosphoric acid containing different concentrations of DEABT.

Table 5
Activation parameters for the corrosion of aged maraging steel in 0.67 M phosphoric acid in the presence of different concentrations of DEABT.

Inhibitor (mM)	E_a (kJ mol^{-1})	$\Delta H^{\#}$ (kJ mol^{-1})	$\Delta S^{\#}$ (J mol^{-1} K^{-1})
0.0	22.42	19.82	−156.42
0.2	38.29	35.69	−112.3
0.4	47.10	44.50	−90.66
0.8	47.79	45.19	−89.99
1.2	48.60	46.00	−89.57

corrosion rate due to the greater area of metal being exposed to the acid [49].

The large negative values of entropy of activation in the absence and presence of inhibitor imply that the activated complex in the rate determining step represents an association rather than dissociation, resulting in a decrease in randomness on going from the reactants to the activated complex [50,51]. The entropy of activation value is higher in the inhibited solutions than that in the uninhibited solution, and the value increases with the increase in the inhibitor concentration. This might be the results of the adsorption of organic inhibitor molecules from the solution which could be regarded as a quasi-substitution process between the organic compound in the aqueous phase and water molecules at the electrode surface [52]. The adsorption of organic inhibitor is accompanied by desorption of water molecules from the surface. Thus the increasing in entropy of activation may be attributed to the increase in solvent entropy [53].

3.5. Adsorption isotherm

The corrosion inhibition actions of organic inhibitors are assigned to their ability to form a protective film between the metal surface and the corrosive medium through their adsorption on the metal/solution interface. The adsorption process of the inhibitor is usually regarded as a substitution process between the organic inhibitor in the aqueous solution [$Inh_{(sol)}$] and water molecules adsorbed at the metal surface [$H_2O_{(ads)}$] as follows [54]:

$$Inh_{(sol)} + \chi H_2O_{(ads)} \leftrightarrow Inh_{(ads)} + \chi H_2O_{(sol)}, \quad (7)$$

where χ represents the number of water molecules replaced by one molecule of the adsorbed inhibitor. The adsorption bond strength is dependent on the composition of the metal, corrosion medium, inhibitor structure, concentration and orientation as well as temperature. The basic information on the interaction between the inhibitor and the alloy surface can be provided by the adsorption isotherm. In order to obtain the adsorption isotherm, the linear relation between surface coverage (θ) value and C_{inh} must be found. The surface coverage θ is given by

$$\theta = \frac{\eta(\%)}{100}, \quad (8)$$

where η% is the percentage inhibition efficiency as calculated using Eq. (2).

Attempts were made to fit the surface coverage (θ) values to various isotherms including Langmuir, Temkin, Frumkin and Flory-Huggins isotherms. By far the best fit was obtained with the Langmuir adsorption isotherm. Langmuir adsorption isotherm for monolayer adsorption is given by the following equation:

$$\frac{C_{inh}}{\theta} = \frac{1}{K_{ads}} + C_{inh}, \quad (9)$$

where C_{inh} is the concentration of inhibitor, K_{ads} is the equilibrium constant for the adsorption process, and θ is the degree of surface coverage which is calculated using Eq. (8).

This model has also been used for other inhibitor systems [54]. The plots of C_{inh}/θ versus C_{inh} gives a straight line with intercept $1/K_{ads}$ as shown in Fig. 6.

The value of standard free energy of adsorption (ΔG^0_{ads}) is related to K_{ads} by the relation (13),

$$\Delta G^0_{ads} = -RT \ln(55.5 K_{ads}), \quad (10)$$

where the value 55.5 is the concentration of water in the solution in mol dm^{-3}, R is the universal gas constant and T is absolute temperature [54].

A plot of ΔG^0_{ads} versus T was used to calculate the standard heat of adsorption, ΔH^0_{ads} and the standard entropy of adsorption, ΔS^0_{ads} according to the thermodynamic Eq. (11) [13].

$$\Delta G^0_{ads} = \Delta H^0_{ads} - T\Delta S^0_{ads} \quad (11)$$

The thermodynamic parameters calculated for the adsorption of DEABT on the alloy surface are tabulated in Table 6. The correlation coefficient (R^2) was used to choose the isotherm that best fit the experimental data [37]. The linear regression coefficient values

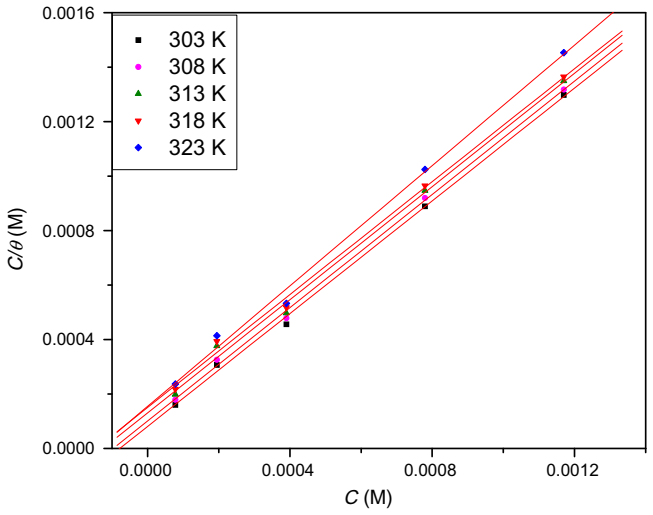

Fig. 6. Langmuir adsorption isotherm for the adsorption of DEABT on aged maraging steel surface in 0.67 M phosphoric acid at different temperatures.

Table 6
Thermodynamic parameters for the adsorption of DEABT on aged maraging steel surface in 0.67 M phosphoric acid.

Temperature (°C)	K (mol^{-1} dm^3)	ΔG^0_{ads} (kJ mol^{-1})	R^2	Slope	ΔH^0_{ads} (kJ mol^{-1})	ΔS^0_{ads} (J mol^{-1} K^{-1})
30	12422	−33.86	0.999	1.04		
35	9910	−33.29	0.999	1.04	−59.47	−85
40	7681	−32.66	0.999	1.04		
45	6667	−32.30	0.999	1.04		
50	6481	−32.23	0.997	1.11		

are close to unity and the slopes of straight lines are nearly unity, suggesting that the adsorption of DEABT obeys Langmuir's adsorption isotherm and there is negligible interaction between the adsorbed molecules [28].

The values of thermodynamic parameters for the adsorption of inhibitors are of significant importance in providing a good insight into the mechanism of corrosion inhibition. In general, an endothermic adsorption process ($\Delta H^0_{ads} > 0$) is attributed unequivocally to chemisorption [55], an exothermic adsorption process ($\Delta H^0_{ads} < 0$) may involve either physisorption or chemisorption or a combination of both the processes. In an exothermic process, the physisorption is distinguished from the chemisorption by considering the absolute values of standard enthalpies of adsorption. The standard enthalpy of a physisorption process is lower than 41.86 kJ mol^{-1}, while that of a chemisorption process approaches to 100 kJ mol^{-1} [56]. In the present case, the calculated value of ΔH^0_{ads} is −59.47 kJ mol^{-1}, which is an intermediate case [57], probably involving both physisorption and chemisorption. Generally, the standard free energy values of −20 kJ mol^{-1} or less negative are associated with physisorption, involving electrostatic interaction between charged molecules and charged metal surface, and those of −40 kJ mol^{-1} or more negative involve charge sharing or transfer from the inhibitor molecules to the metal surface to form a coordinate covalent bond, resulting in chemisorption [58]. The ΔG^0_{ads} values obtained for DEABT on the aged maraging steel surface in 0.67 M phosphoric acid are between −32 and −34 kJ mol^{-1}. These values indicate that the adsorption process may involve complex interactions involving both physical and chemical adsorption of the inhibitor, as reported by Li et al. [28]. The fact that both ΔG^0_{ads} and inhibition efficiency decrease with the increase in temperature, indicates that the adsorption of DEABT on the maraging steel surface in phosphoric acid are not favored at high temperature and hence can be considered to be predominantly physisorption.

The ΔS^0_{ads} value is large and negative; indicating that decrease in disordering takes place on going from the reactant to the alloy adsorbed species. This can be attributed to the fact that adsorption is always accompanied by decrease in entropy.

3.6. Mechanism of corrosion inhibition

Aged maraging steel results from the precipitation of inter-metallics. Since these inter-metallics have different composition, their electrochemical behavior is expected to be different from that of the matrix [59]. Also, there will be strain fields around these coherent precipitates as a result of lattice mismatch between the precipitate and the matrix due to the difference in the crystal structure and lattice parameters. These strain fields in combination with the galvanic effect due to the composition difference leads to the enhanced corrosion of aged maraging steel in acid medium. Considering the inhomogeneous nature, the surface of the alloy is generally characterized by multiple adsorption sites having different activation energies and enthalpies of adsorption. Inhibitor molecules may thus be adsorbed more readily at surface active sites having suitable adsorption enthalpies.

In order to predict the mechanism of inhibition, the interaction between the inhibitor compound and the metal surface must be known. Many organic corrosion inhibitors have at least one polar unit with a hetero atom; this polar unit is regarded as the reaction center for the adsorption process. Furthermore, the size, orientation, shape and electric charge on the molecule determine the degree of adsorption and hence the effectiveness of inhibitor. For instance sulfur containing substances have been shown to preferentially chemisorb on the surface of iron in acidic medium, whereas nitrogen containing substances tend to favor physisorption [60]. It is reported that protective values of sulfur containing compounds are superior to that of nitrogen containing compounds. This may be due to the greater polarizability of sulfur atom and the presence of two electron pairs available for co-ordination [24]. On the other hand, iron is well known for its coordination affinity to ligands possessing heteroatom. Increase in inhibition efficiencies with increase in inhibitor concentration shows that the inhibition action is due to the adsorption on the maraging steel surface. Four types of adsorption may take place by organic molecules at metal/solution interface namely,

1. Electrostatic attraction between the charged molecules and charged metal.
2. Interaction of unshared electron pairs in the molecule with the metal.
3. Interaction of π-electrons with the metal.
4. Combination of (1) and (3) [61].

At the interface of iron and acid electrolyte, the dissolution of iron can be written as follows [62]:

$$Fe + H_2O \iff FeOH_{ads} + H^+ + e^- \quad (12)$$

$$FeOH_{ads} \rightarrow FeOH^+ + e^- \quad (13)$$

$$FeOH^+ \iff Fe^{2+} + OH^-. \quad (14)$$

At medium and high concentrations of phosphoric acid, precipitation of iron phosphate occurs at the interface [63] as follows:

$$6H_3PO_4 + 3Fe \rightarrow 3Fe(H_2PO_4)_2 + 3H_2 \quad (15)$$

$$3Fe(H_2PO_4)_2 \rightarrow Fe_3(PO_4)_2 + 4H_3PO_4 \quad (16)$$

However, this precipitation can be weakly observed when steel is treated with phosphoric acid solutions of low concentrations [63]. The present study deals with low concentration of phosphoric acid and the inhibition effect of DEABT in the phosphoric acid solution can be explained as follows.

In aqueous acidic solution, DEABT exists partly in the form of protonated species and partly as neutral molecules. Generally two modes of adsorption could be considered. It is well known that steel surface bears a positive charge in acid solutions [38,64,65]. According to L. Wang [65] although the potential at zero charge (*PZC*) is not available for steel in H_3PO_4, it may be considered that the adsorption of phosphate ions displace *PZC* to the more positive value than E_{corr} for steel in phosphoric acid. This would make the steel surface negatively charged and susceptible to physical adsorption of positively charged inhibitor species [66]. Therefore,

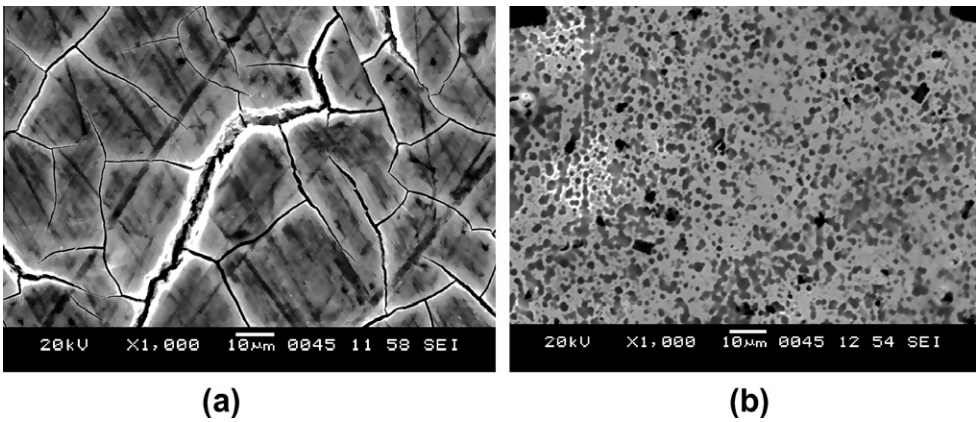

Fig. 7. SEM images of the surfaces of aged maraging steel after immersion in 0.67 M phosphoric acid: (a) in the absence and (b) in the presence of DEABT.

the adsorption of protonated species would be through electrostatic attraction between the positively charged inhibitor molecule and the negatively charged phosphate ions adsorbed on the metal surface, resulting in physisorption. The neutral inhibitor molecules may occupy the vacant adsorption sites on the metal surface through the chemisorption mode involving the displacement of water molecules from the metal surface and sharing of electrons by the hetero atoms like nitrogen and/or sulfur with iron. Chemisorption is also possible by the donor–acceptor interactions between π electrons of the aromatic ring and the vacant d orbitals of iron, providing another mode of protection [38,66]. Thus DEABT molecules anchor to the alloy surface through the protonated nitrogen atom resulting in physisorption and through the sulfur and/or aromatic benzene ring resulting in chemisorption.

3.7. Scanning electron microscope (SEM) studies

The surface morphology of the aged samples was examined by SEM immediately after the sample is subjected to corrosion tests in H_3PO_4 medium in the absence and in the presence of inhibitor. The SEM image of the surface of the corroded aged maraging steel sample in Fig. 7a shows degradation of alloy in phosphoric acid in the absence of inhibitor. The attack by H_3PO_4 is seen to be more at grain boundary since these regions are highly susceptible to corrosion. In aged samples the intermetallic precipitation at grain boundary may be responsible for the higher rate of corrosion. Fig. 7b represents the SEM image of the aged maraging steel after the corrosion tests in a medium of phosphoric acid containing DEABT. The image clearly shows the adsorbed layer of inhibitor molecules on the alloy surface thus protecting the metal from corrosion.

4. Conclusions

The corrosion of aged maraging steel in 0.67 M phosphoric acid is significantly reduced by the addition of DEABT. The inhibition efficiency of DEABT increases with the increase in the inhibitor concentration and decreases with the increase in temperature of the corrosion medium. Energy of activation for the corrosion process increases in the presence of inhibitor. DEABT acts as a mixed type inhibitors, affecting both anodic and cathodic corrosion reaction rates. The adsorption of DEABT on the aged maraging steel surface obeys Langmuir's adsorption isotherm model. The variation of inhibition efficiency with temperature and the values of ΔG^0_{ads} and ΔH^0_{ads} predict both physisorption and chemisorption of DEABT on the alloy surface, but predominantly physisorption.

References

[1] K.Y. Sastry, R. Narayanan, C.R. Shamantha, S.S. Sunderason, S.K. Seshadri, V.M. Radhakrishnan, K.J.L. Iyer, S. Sundararajan, Mater. Sci. Technol. 19 (2003) 375–381.
[2] K. Rohrbach, M. Schmidt, ASM Handbook, 10th ed., vol. 1, ASM International, 1990. pp. 796.
[3] D.G. Lee, K.C. Jang, J.M. Kuk, I.S. Kim, J. Mater. Process. Technol. 62 (2005) 342–349.
[4] W.W. Krick, R.A. Covert, T.P. May, Met. Eng. Quart. 8 (1968) 31–33.
[5] S.W. Dean, H.R. Copson, Corrosion 21 (1965) 95–98.
[6] G. Bellanger, J.J. Rameau, J. Nucl. Mater. 228 (1996) 24–37.
[7] G. Bellanger, J. Nucl. Mater. 217 (1994) 187–193.
[8] Data Bulletin on 18% Ni Maraging Steel (1964), The International Nickel Company, INC.
[9] J. Rezek, I.E. Klein, J. Yhalom, Corros. Sci. 39 (1997) 385–397.
[10] V.S. Muralidharan, K.S. Rajagopalan, Corros. Sci. 19 (1979) 199–207.
[11] T. Poornima, J. Nayak, A.N. Shetty, Int. J. Electrochem. Sci. 5 (2010) 56–71.
[12] T. Poornima, J. Nayak, A.N. Shetty, J. Appl. Electrochem. 41 (2011) 223–233.
[13] F. Bentiss, M. Lebrini, M. Lagrenee, Corros. Sci. 47 (2005) 2915–2931.
[14] M. Lebrini, F. Bentiss, H. Vezin, M. Lagrenée, Corros. Sci. 48 (2006) 1279–1291.
[15] S. Sankarapapavinasam, F. Pushpanaden, M.F. Ahmed, Corros. Sci. 32 (1991) 193–203.
[16] G. Schmitt, Br. Corros. J. 19 (1984) 165–169.
[17] S. Singh, F. Athar, A. Azam, Bioorg. Med. Chem. Lett. 15 (2005) 5424–5428.
[18] B.O. Renata, M.S.F. Elaine, P.P.S. Rodrigo, A.A. Anderson, U.K. Antoniana, L.Z. Carlos, Eur. J. Med. Chem. 43 (2008) 1983–1988.
[19] J. Easmon, G. Heinisch, W. Holzer, B. Rosenwirth, J. Med. Chem. 35 (1992) 3288–3296.
[20] O.E. Offiong, S. Martelli, Il Farmaco 42 (1992) 1543–1548.
[21] O.E. Offiong, S. Martelli, Il Farmaco 48 (1993) 777–782.
[22] S.T. Arab, Mat. Res. Bull. 43 (2008) 510–521.
[23] B.A. Abd El-Nabey, E. Khamis, G.E. Thompson, J.L. Dawson, Surf. Coat. Technol. 28 (1986) 83–91.
[24] E.E. Ebenso, U.J. Ekpe, B.I. Ita, O.E. Offiong, U.J. Ibok, Mat. Chem. Phys. 60 (1999) 79–90.
[25] K.S. Jacob, G. Parameswaran, Corros. Sci. 52 (2010) 224–228.
[26] P.T. Shah, T.C. Daniels, Rev. Trav. Chim. 69 (1950) 1545–1549.
[27] D. Jayaperumal, Mater. Chem. Phys. 119 (2010) 478–484.
[28] W. Li, Q. He, S. Zhang, C. Pei, B. Hou, J. Appl. Electrochem. 38 (2008) 289–295.
[29] C. Cao, Corros. Sci. 38 (1996) 2073–2082.
[30] M. Ehteshamzadeh, A.H. Jafari, E. Naderi, M.G. Hosseini, Mater. Chem. Phys. 113 (2009) 986–993.
[31] B.G. Ateya, M.B.A. El-Khair, I.A. Abdel-Hamed, Corros. Sci. 16 (1976) 163–169.
[32] E. McCafferty, N. Hackerman, J. Electrochem. Soc. 119 (1972) 146–154.
[33] A.A. Aksut, W.J. Lorenz, F. Mansfeld, Corros. Sci. 22 (1982) 611–619.
[34] M.A. Amin, S.S. Abd El-Rehim, E.E.F. El-Sherbini, R.S. Bayoumi, Electrochim. Acta 52 (2007) 3588–3600.
[35] S. Cheng, S. Chen, T. Liu, X. Chang, Y. Yin, Electrochim. Acta 52 (2007) 5932–5938.
[36] N. Labjar, M. Lebrini, F. Bentiss, N.E. Chihib, S. El Hajjaji, C. Jama, Mater. Chem. Phys. 119 (2010) 330–336.
[37] I. Ahamad, R. Prasad, M.A. Quraishi, Corros. Sci. 52 (2010) 1472–1481.
[38] M.A. Veloz, I. Gonzalez, Electrichim. Acta 48 (2002) 135–144.
[39] E.M. Sherif, S.M. Park, Electrochim. Acta 51 (2006) 1313–1321.
[40] M.A. Amin, K.F. Khaled, S.A. Fadl-Allah, Corros. Sci. 52 (2010) 140–151.
[41] A. Popova, E. Sokolova, S. Raicheva, M. Christov, Corros. Sci. 45 (2003) 33–58.
[42] E. Barsoukov, J.R. Macdonald, Impedance Spectroscopy Theory, Experiment, and Applications, second ed., John Wiley & Sons, New Jersey, 2005. pp. 494.
[43] A. El-Sayed, J. Appl. Electrochem. 27 (1997) 193–200.
[44] H.H. Hassan, E. Abdelghani, M.A. Amin, Electrochim. Acta 52 (2007) 6359–6366.

[45] M.M. Solomon, S.A. Umoren, I.I. Udosoro, A.P. Udoh, Corros. Sci. 52 (2010) 1317–1325.
[46] L.I. Antropov, Corros. Sci. 7 (1967) 607–620.
[47] E.E.F. El Sherbini, Mater. Chem. Phys. 60 (1999) 286–290.
[48] T. Szauer, A. Brand, Electrochim. Acta 26 (1981) 1253–1256.
[49] M.K. Gomma, M.H. Wahdan, Mater. Chem. Phys. 39 (1995) 209–213.
[50] J. Marsh, Advanced Organic Chemistry, third ed., Wiley Eastern, New Delhi, 1988.
[51] M. Sahin, S. Bilgic, H. Yilmaz, Appl. Surf. Sci. 195 (2002) 1–7.
[52] B. Ateya, B.E. El-Anadouli, F.M. El-Nizamy, Corros. Sci. 24 (1984) 509–515.
[53] E.E. Oguzie, V.O. Njoku, C.K. Enenebeaku, C.O. Akalezi, C. Obi, Corros. Sci. 50 (2008) 3480–3486.
[54] M. Hosseini, S.F.L. Mertens, M.R. Arshadi, Corros. Sci. 45 (2003) 1473–1489.
[55] S. Martinez, I. Stern, Appl. Surf. Sci. 199 (2002) 83–89.
[56] A.K. Singh, M.A. Quraishi, Corros. Sci. 52 (2010) 152–160.
[57] D.W. Shoesmith, Metals Handbook, ninth ed., vol. 13, ASM International, 1992, p. 18.
[58] W. Durnie, R.D. Marco, A. Jefferson, B. Kinsella, J. Electrochem. Soc. 146 (1999) 1751–1756.
[59] A. Fragnani, G. Trabanelli, Corrosion 55 (1999) 653–660.
[60] H. Shorky, M. Yuasa, I. Sekine, R.M. Issa, H.Y. El-baradie, G.K. Gomma, Corros. Sci. 40 (1998) 2173–2186.
[61] D. Schweinsgberg, G. George, A. Nanayakkawa, D. Steinert, Corros. Sci. 28 (1988) 33.
[62] J.O.M. Bockris, M.A.V. Devanathan, K. Muller, Proc. R. Soc. A274 (1963) 55.
[63] G.N. Mu, T.P. Zhao, M. Liu, T. Gu, Corrosion 52 (1996) 853–856.
[64] G.N. Mu, X.M. Li, F. Li, Mater. Chem. Phys. 86 (2004) 59–68.
[65] L. Wang, Corros. Sci. 43 (2001) 2281–2289.
[66] A.K. Satpati, P.V. Ravindran, Mater. Chem. Phys. 109 (2008) 352–359.